MRI investigation of swelling of super absorbent polymer: effects of particle size

Citation for the original published paper (version of record):
Tiernan, H., Khoshhal Salestan, S., Baena-Moreno, F. et al (2026). MRI investigation of swelling of super absorbent polymer: effects of particle size. Journal of Materials Science, 61(19): 13701-13715. http://dx.doi.org/10.1007/s10853-026-12659-2

J Mater Sci (2026) 61:13701–13715

Polymers & biopolymers

MRI investigation of swelling of super absorbent polymer: effects of particle size

Hannah Tiernan[1], Saeed Khoshhal Salestan[1], Francisco Manuel Baena-Moreno[3], Ramin Moghadasi[2], Tomas Karlson[2], Charlotta Hanson[1,2], and Diana Bernin[1,*]

[1] *Chalmers University of Technology, Gothenburg, Sweden*
[2] *Essity, Mölndal, Sweden*
[3] *University of Seville, Seville, Spain*

Received: 10 October 2025
Accepted: 23 March 2026
Published online: 5 April 2026

ABSTRACT

Superabsorbent polymers (SAP) are crucial components of hygiene products. Their method of manufacture, particle size, and the presence of ions enable the performance of SAP to be tailored towards different applications. The efficacy of their function could be attributed to the distribution of H_2O molecules within the sample, e.g. transporting the liquid away from the skin. We therefore aim to further elucidate this process using magnetic resonance imaging (MRI). Here we utilisized MRI techniques, relaxation times, diffusion coefficient measurements and 1D profiling, to investigate the distribution of H_2O molecules in SAPs while varying particle size and the presence of NaCl in the solution to be absorbed. Through detailed analysis of the MRI results, factors such as the pushed height of the plunger, spatial swelling heterogeneity, and the swelling of the SAP particles could be monitored. As expected, SAP particles swelled less in saline solution. The H_2O absorption appeared the most homogenous for the smallest particle size. It shows, in a comparable manner, the position of water and its state in terms of being free or strongly associated. The analytical measures and representative maps of fluid distribution were proved to shed light on fluids absorption in a bed of gelling particles. The results suggest that a homogeneous swelling and a faster H_2O absorption might occur with smaller SAP particles. These findings provide valuable insights into fluid transport and mechanical response in SAPs, which are critical for optimising their application in hygiene products.

Handling Editor: Gregory Rutledge.

Address correspondence to E-mail: diana.bernin@chalmers.se

https://doi.org/10.1007/s10853-026-12659-2

GRAPHICAL ABSTRACT

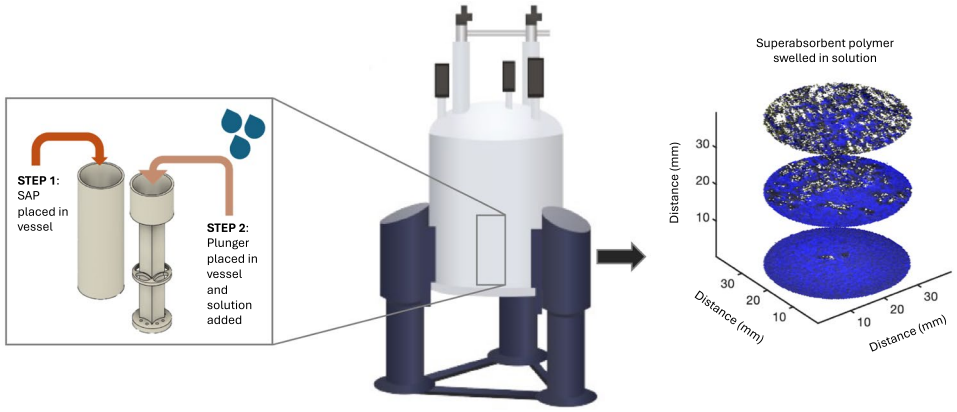

Introduction

SAPs have numerous applications, from concrete curing [1] and medicine [2], to agricultural production [3] and hygiene products [4]. The global SAP market was estimated at USD 6.49 Bn in 2023, with hygiene products—including nappies, taking over 65% of this share [5]. Common commercial SAPs are made from poly(acrylic acid) and its salts, and their main property is their ability to retain liquid many times their original weight [6]. The swelling process of SAP can be divided into three main stages: firstly, H_2O absorption, when the hydrophilic groups in the polymer chains attract and associate with H_2O molecules; secondly, polymer network expansion, when the cross-linked structure of the polymer allows it to retain H_2O molecules while maintaining its shape, and the polymer swells as the H_2O molecules enter the network; and finally, equilibrium state, here the polymer network reaches a balance between the osmotic pressure and the elastic restoring forces of the polymer chains. The polymer subsequently holds the absorbed H_2O in a gel-like state [7]. It is important to note that sodium or other ions present in the SAP or in the solution play an important role in this process.

Nuclear magnetic resonance (NMR) encompasses both spectroscopic and imaging techniques, each with distinct analytical applications. NMR spectroscopy provides high spectroscopic resolution, resolving molecular structure and chemical environments, while low-field NMR and similar methods measure bulk relaxation and diffusion without spectroscopic detail. When spatial resolution is introduced, the technique is termed NMR imaging, though magnetic resonance imaging (MRI) is the preferred term in biomedical and material sciences. Unlike NMR spectroscopy, MRI visualises structural and compositional heterogeneity by mapping for example relaxation times and diffusion properties, highlighting the diverse applications of NMR-based techniques [8]. Magnetic resonance imaging (MRI) is a non-invasive and non-destructive tool, which can be utilised in numerous applications, including those in biochemistry and chemical engineering, as well as biomedical studies [9–11]. MRI requires minimal sample preparation and provides high-resolution and time-resolved measurements, making it suitable for investigation of processes resulting in a physical or chemical change. By employing MRI techniques, relaxation times, and diffusion coefficient measurements, researchers can non-invasively study the interactions between H_2O and polymer networks.

Initial studies of SAPs using NMR were carried out in the late 1990's [12], and since then, other SAP and NMR research has been conducted, particularly in the field of concrete curing [1, 13]. SAP structural parameters have also been investigated using NMR and solid-state ^{13}C NMR [14–16]. Studies of SAP in hygiene products utilise a variety of testing methods. For example, to test absorbency of SAP in hygiene products, it is common to employ absorption testing methods whereby samples are weighed before and after swelling [4, 17]. These techniques are useful and provide essential information about the overall absorption performance. However, important information is missing—the location of the fluid within the

sample cannot be visualised. It is therefore unclear whether the fluid at different positions is strongly associated with the SAP or free in the porous structure outside the particles. This distribution may depend on particle size and mechanical load. In addition, Fourier transform infrared (FTIR), scanning electron microscopy (SEM), and X-ray diffraction (XRD) are often used for characterisation of SAPs [18–20], but do not offer spatially resolved images of the water location, which is fundamental for many applications. Pivotal work by Blumich et al. [21] used NMR MOUSE to investigate and quantify liquid properties in fibrous, porous materials, obtaining spatial information in one dimension, primarily to understand how weakly or strongly associated fluids affect relaxation times. As an example, one of their key findings was the observation of major differences in liquid distributions and flow dynamics between one 400 μm thick fibrous layer, and two stacked 200 μm thick fibrous layers of the same material [21, 22].

MRI is a good alternative to NMR for studying SAPs due to its ability to provide spatially resolved, real-time tracking of swelling processes. Although the direct results of this study are specific to the SAP that has been investigated, the methodology can be utilised in the future for investigation of a wide variety of SAPs and fluids. Previous research employing MRI to examine superabsorbent polymers in hygiene products remains limited. However, one study used MRI to examine water distribution and mobility in disposable incontinence pads, finding that superabsorbent polymers strongly retain water with restricted mobility, while fluffed wood pulp holds water more loosely, allowing for greater exchange and diffusion [23]. Another study used MRI to analyse biobased hydrogel polymer matrices [24].

Absorption capacity of saline is consistently listed as one of the top attributes for SAP materials [2, 17, 25, 26]; therefore, this research has specifically explored swelling of SAP when comparing saline solution with water. Previous studies have shown that an increase in NaCl concentration leads to a decrease in swelling ratio. However, this has been done using methods showing the overall absorption capacity of the superabsorbent, without visualising the fluid distribution in the swelled structure [27, 28]. In the present study, saline solution or water was added top wise on a bed of SAP particles of varying sizes under an applied load (plunger), and the distribution of H_2O molecules was subsequently monitored using MRI. Hence, the research question we aim to answer is: does saline introduce heterogeneity in swelling and water distribution in superabsorbent polymers, and can this be visualised with MRI?

This work is structured as follows: first, we present the methodology, detailing the experimental setup and measurement parameters. Next, we analyse the swelling behaviour and pushed height of swelled SAPs (which corresponds here to the distance the plunger is raised in each experiment) using normalised D and T_2 maps and distribution plots. The progress of swelling was followed using 1D ^{1}H profiling. Finally, we explore SAP heterogeneity by examining three of the four statistical moments of distribution, providing deeper insights into the absorption of aqueous and saline solution. Overall, we aim to explain how MRI analysis of normalised apparent diffusion coefficient D and relaxation time T_2 maps can be used to illustrate differences in pushed height as a proxy of swelling of SAP particles.

Material and methods

Sample preparation

SAP of sizes: 150–300 μm, 300–600 μm, and 'whole fraction' (containing a full range of typical hygiene product particle sizes from 50 μm–1 mm) were used (Essity, Sweden), referred to herein as SAP1, SAP2, and SAP3. Each of these sample sizes was weighed out at 0.2, 0.3, and 0.4 g, and 10 ml of either distilled H_2O or 0.9 wt% NaCl solution (referred to henceforth as 'saline') was added to give ratios of 1:50, 1:33, and 1:25, respectively. All samples were left to equilibrate in the MRI probe for 2 h before measurement. It can be assumed that samples have reached equilibrium after two hours [29]. All experiments were completed within 24 h of sample preparation. The gradient coil, which surrounds the sample, is water cooled, and the temperature of the water bath was set to 25 °C.

Magnetic resonance imaging (MRI)

Magnetic resonance imaging (MRI) experiments were performed on a WB400 Bruker Avance III HD spectrometer (^{1}H Larmor frequency—300 MHz), equipped with a 40 mm probe. The field of view was set to 40 × 40 mm^2, and 128 × 128 points were recorded, yielding a

spatial resolution of each voxel of 312.5 × 312.5 μm^2 with a slice thickness of 1 mm.

All slices were axial or sagittal slices measured without a slice gap and in an interleaved order. The slice thickness of 1 mm remained the same, but the exact positions and numbers of slices measured, typically between 7 and 14, changed according to swelling of the sample, to measure the total swelled area. All axial slices throughout the sample were analysed to find the true top, middle, and bottom slices. Axial slices were taken for further analysis from top minus 1 slice to negate impact of the plunger or air inclusions on the top of the sample.

The 1D ^{1}H spin-echo based profiles were recorded in 5 sagittal slices with a thickness of 1 mm throughout the sample using a repetition time of 120 ms and an echo time of 5.02 ms with a spatial resolution of 0.351 mm. The preparation of the sample was as follows: 0.3 g of SAP1, SAP2, and SAP3 was added in a plastic vial. 10 ml of water or saline was added, and then, the sample was immediately mounted in the MRI and the measurements were started at the same time. The temporal resolution is 130 ms, and the experiment was repeated 5000 times. Dummy scans were used to minimise T_1-weighting. The profiles were evaluated through measuring the total height of the sample for each experiment using MATLAB and own scripts.

MRI sample holder

A schematic diagram of the sample holder is shown in Fig. 1. It was 3D-printed in-house using a Formlabs printer, in Formlabs Grey Resin. 0.2, 0.3, or 0.4 g of SAP was placed at the bottom of the cylindrical vessel, a plunger weighing 34.83 g was placed over the SAP sample, and then 10 ml of distilled H_2O, or saline was added evenly, top wise, via a syringe connected to a tubing. The holes in the bottom plate of the plunger allowed for an even distribution of liquid over the SAP particles. The plunger was designed to enable additional weight to be applied during swelling, which will be explored in a later study.

Spin–spin relaxation (T_2) maps

T_2 maps were used to monitor changes in the swelling of SAP. The Paravision method MSME (Multiple Slice Multiple Echo) was applied with an echo spacing of 15 ms. 64 equally spaced echo times, t_e, from 15 ms up to 960 ms, were used to extract ^{1}H T_2 for each voxel. The total experiment duration varied due to repetition time. The repetition time ranged from 4 to 15 s, and the position and the number of slices were adjusted as mentioned in 2.1. The T_2 in each voxel was obtained by fitting the signal I_{te} using the following equation $I_{te} = I_{0te}\exp(-t_e/T_2)$ with I_{0te} being the initial intensity at $t_e = 0$. The obtained T_2 was normalised with the T_2 for water or saline. The fitting procedure was performed in MATLAB using own scripts.

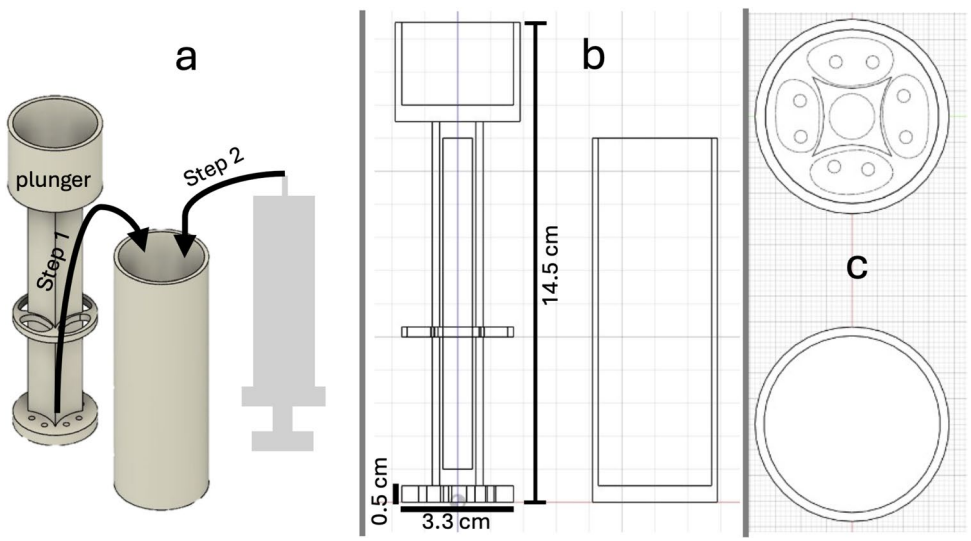

Figure 1 3D-printed sample holder, **a** solid render indicating the plunger. step 1: SAP sample is deposited in container, and plunger is then placed on top; step 2: syringe connected to tubing is then used to add solution over the holes in the plunger. **b** sagittal line drawing, **c** axial line drawing (top, plunger, bottom, sample holder)

Diffusion coefficient (D) maps

The diffusion tensor imaging method DtiStandard produces images which are sensitised to the molecular diffusion of H_2O [30], and the signal displayed corresponds to the random movement of H_2O protons. The DtiStandard method was utilised to extract the diffusion coefficient denoted D. A repetition time of 1000 ms and 16 b values were used. The gradient duration ∂ (4 ms) and diffusion time Δ (10 ms) resulted in effective b values from 14.40 up to 5756.54 s/mm^2. The position and the number of slices were adjusted as mentioned in 2.1. The diffusion coefficient D and the initial intensity I_{0D} at the diffusion gradient strength = 0 were estimated using the obtained signal I_D and the following equation $I_D = I_{0D}\exp(-bD)$ as a function of the diffusion weighting variable b. The obtained diffusion coefficient D was normalised with the diffusion coefficient of water or saline, respectively. The fitting procedure was performed in MATLAB using custom scripts developed for this study.

Results and discussion

Swelling of SAP

Figure 2a displays sagittal middle slices of normalised D and T_2 maps derived from a series of MRI images weighted by the b values or the echo time t_e, and overlayed maps of both. The fitted diffusion coefficients D and the relaxation times T_2 were normalised by the diffusion coefficient of H_2O in saline solution or water, and the T_2 relaxation time of H_2O in saline solution or water, respectively. From here on, all reported Ds and T_2s refer to the normalised Ds and T_2s (note that the 's' denotes plural of D and T_2). The diffusion coefficient D highlights the movement or restriction of H_2O molecules within the polymer network and is more sensitive to the SAP polymer network structure and cross-linking. D can also distinguish between the sizes of the voids between the cross-links or the network. However, due to limitations of the technique, an H_2O molecule might only diffuse tens of µms for water during the diffusion time to probe the voids. Therefore, for larger voids on a mm scale, the observed D would correspond to free diffusion [31]. A value close to 1 for normalised D indicates that the H_2O molecules diffuse freely, 0.5 indicates slower diffusion, and 0.1 slow diffusion. While for T_2 a value close to 1 indicates that the H_2O molecules are less associated with the SAP molecules, 0.5 would indicate stronger association, and 0.1 stronger association still, in comparison with free H_2O molecules.

Figure 2a displays sagittal D maps of 0.3 g SAP2 for water (top) and saline solution (bottom). In both cases, SAP particles are found above the bottom plate of the plunger (see Fig. 1 for the position of

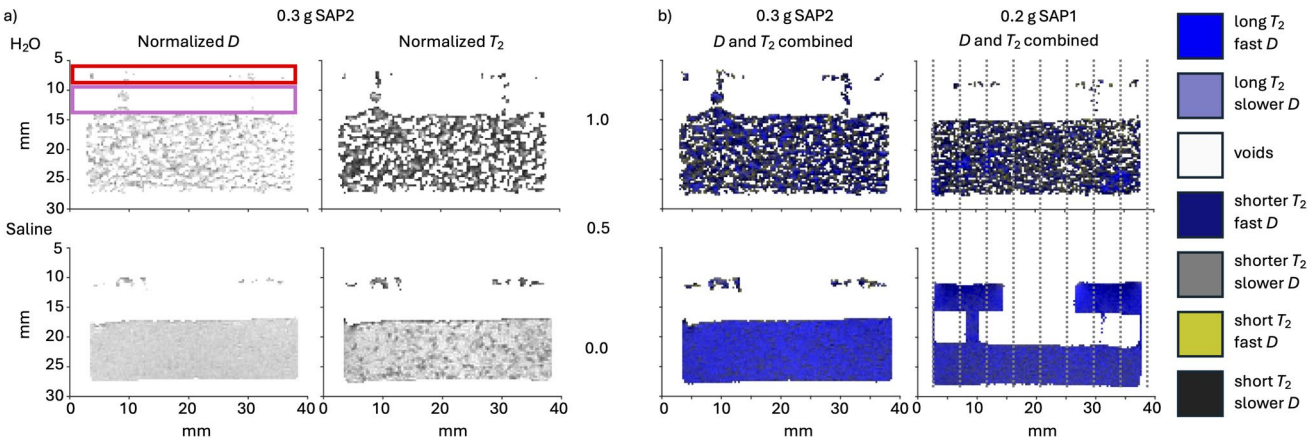

Figure 2 Example sagittal slices of normalised D, normalised T_2 and D and T_2 combined for **a** 0.3 g SAP2 in water (top) and saline (bottom), **b** 0.2 g SAP1 in water (top) and saline (bottom); red box indicates area referred to as 'solution on top of bottom plate of the plunger', purple box indicates 'plunger bottom plate'; measurements normalised to either water or saline solution and scale bar refers to diffusion and normalised T_2 values with a value closer to 1 indicating that the H_2O diffuses freely, and that the H_2O molecule is less strongly associated with the SAP molecules, while a value around 0.1 would indicate slow diffusion; dashed lines in **b** indicate the estimated position of the pushed height

the plunger). In the *z*-direction, both *D* and T_2 maps show larger swelling of the SAP in water compared to saline. The voids in the maps, i.e. the regions without a *D* or T_2 value (white areas), result from the formation of air gaps between the swelled SAP particles. The swelling is less pronounced in the saline solution sample, and no voids were detected. Comparing diffusion coefficients, the H_2O diffusion appears similar, independent of the presence of salt in water (albeit there are small regions present in which the H_2O molecules diffuse slower in the SAP sample swelled with water). T_2 is sensitive to the pore size and interactions with the surface of the porous materials [32]. From previous research, it is well known that labile hydrogens on COOH/COO^- groups exchange with the hydrogens on the H_2O [33]. As it is dependent on the rate of exchange, the T_2 can be impacted and subsequently shortened. This could explain the lower T_2 values for SAP swelled in water. In the presence of saline, sodium ions in solution and those associated with SAP polymer chains will compete with the H_2O molecules for the negatively charged COO^- sites which may alter the exchange rate. Therefore, T_2 might show lower values when the SAP is swollen with water compared to saline, due to increased swelling and accessible COO^- groups. Pell et al. used 1 g SAP per 10 ml H_2O, or 10 wt% NaCl. They observed a similar T_2 for both cases (which after normalisation was 0.5), and used a range of experimental settings including a longer echo time and varying liquid to SAP ratios and concentrations, which could complicate a direct comparison [23]. However, we found similar values to Pell et al. for some SAP samples swelled in water.

D and T_2 maps, which illustrate H_2O transport and H_2O interaction, respectively, are overlayed in Fig. 2b to provide more detailed information about H_2O behaviour in SAP, which is dependent on the SAP content and the presence of sodium ions in solution. The colour encoding key is found to the right. 0.3 g SAP2 swelled with water is demonstrated by some bright blue coloured regions which show H_2O molecules with a long T_2 and fast diffusion. These could either be regions with highly swelled SAP particles, or regions of H_2O molecules between particles which may have saturation of particles or perhaps gel blocking [34]. Most other regions are grey, yellow, and black, suggesting that both T_2 and *D* are reduced. This could result from less swelled particles in which the H_2O diffusion is slightly restricted, and where H_2O can exchange with the COOH/COO^- groups on the SAP polymer. The corresponding saline swelled sample with the same particle size (either SAP1 or SAP2) and SAP concentration appears homogenous indicating H_2O being present between the particles and inside the swelled particles. There are no visible voids and most of the H_2O appears to be fast diffusing with a long T_2, albeit with less swelling. There are also some grey areas, indicating H_2O molecules with shorter T_2 and slower *D*, respectively. The grey areas demonstrate areas of less swelled SAP. The T_2 is most likely less impacted by the hydrogen exchange due to the sodium or other ions present in the SAP.

From the sagittal images, additional information like the distance that the plunger was pushed due to the swelling can be denoted as the pushed height. The mechanical work carried out by the swelling of the SAP has been used as an osmotic engine [35, 36]. The lower SAP concentration with a smaller particle size (SAP1) produces visible voids and blue regions in the maps in Fig. 2b (right, top). For the saline sample, part of the liquid and SAP particles moved upwards through the holes on top of the bottom plate of the plunger, indicating that the saline solution has not been absorbed completely in Fig. 2b (right, bottom). The pushed height is almost halved for this sample. A higher concentration of SAP and a larger particle size (SAP2) result in only a slightly increased SAP pushed height for H_2O in Fig. 2b (left, top) while for the corresponding saline sample most of the SAP particles stayed below the bottom plate.

As previously explained, pushed height within our setup was calculated from the sagittal images, and the positions are illustrated by the grey dashed lines in Fig. 2b. Due to the sample holder design, and as seen in Fig. 2b (bottom), some liquid and SAP particles might also be on top of the bottom plate of the plunger. This phenomenon was observed for all samples. We therefore estimated the pushed height below the plunger (light blue), and the height including the liquid, the bottom plate, and the SAP particles on the top of the bottom plate (dark blue) are shown in Fig. 3. At all concentrations and particle sizes (SAP1, SAP2, and SAP3), pushed height is higher with H_2O than with saline solution. This phenomenon has been observed previously [37, 38], but here it has been visualised using MRI. Then, on moving to higher SAP concentrations, for H_2O, the pushed height became slightly larger due to more SAP being present in contrast to the saline samples showing a clear increase with higher SAP

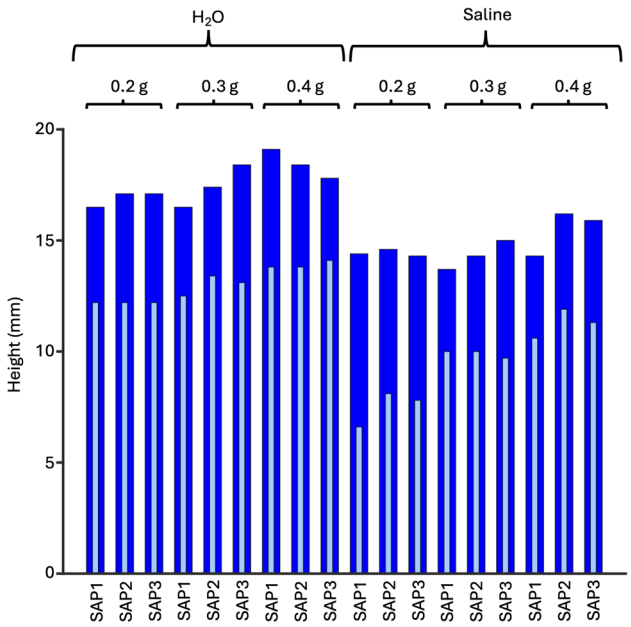

Figure 3 Pushed height (light blue) and the overall height including the fluid/SAP particles on top of the bottom plate (dark blue), of 0.2, 0.3, and 0.4 g and SAP1, SAP2, and SAP3, in either H_2O or saline solution

concentrations. The differences between the pushed height and the overall height, including the fluid on the top of the bottom plate, appeared similar for H_2O. The largest difference was found for the lowest SAP concentration for saline samples. With our settings and experimental setup, we could not see evidence that the pushed height nor SAP on the top of the bottom plate is affected by the particle size.

Swelling heterogeneity of swelled SAP

Sagittal images provide little information about the axial distribution. The critical question raised is then: do SAPs swell hetero- or homogenously, and what does the resulting fluid distribution look like? In this section, we address this question by determining the location of H_2O molecules in swelled SAP in either water or saline solution. We use axial slices, distributions derived from the axial slices, and moments of these distributions to investigate heterogeneity in all samples.

To determine the location of H_2O within swelled SAP samples, we use overlayed T_2 and D maps of single axial slices, as shown in Fig. 4. These are categorised according to SAP concentration, solution type, and SAP particle size (SAP1, SAP2, or SAP3). The diffusion coefficient D and the T_2 were normalised according to the procedure outlined in Sect. "MRI sample holder" and "Spin–spin relaxation (T2) maps".

Overlayed D and T_2 maps show increased swelling of SAP in water compared to saline, indicated by voids and the lack of many bright blue regions (Fig. 2). Formed voids are much more visible in H_2O swelled SAP than saline. By using the colour key in Fig. 4, it is evident that bottom slices for saline samples appear in a slightly darker blue which is attributed to shorter T_2 values compared to the top slice. However, an interesting heterogeneity can be seen between the top slices of the saline swelled SAP, particularly at 0.4 g SAP concentration. Hence, once the water or saline solution is added to the SAP and the particles have swollen above the remaining liquid, H_2O molecules are not transported upwards again towards the upper layers. This is relevant to the application of SAPs in hygiene products, where it is essential that liquid is moved away from the surface in contact with the skin. Instead of showing regions dominated by a bright blue colour, indicating long T_2 and fast D, there are grey and black colours showing shorter and short T_2 and slower D, respectively.

Less swelled SAP particles should have smaller voids between the SAP polymer chains inside a particle, resulting in slower H_2O diffusion. However, we observed predominantly fast diffusion in SAP samples swelled in saline solution which could be due to two reasons. Firstly, during the diffusion time set in the experiment, H_2O molecules diffuse both within the less swelled particle and between the voids. This leads to an average diffusion coefficient which is weighted by the fast-diffusing H_2O molecules leading to a faster D which is slightly slower compared to D of the reference, the saline solution. A second, less likely reason, could be that the T_2 of H_2O in the less swelled particles is very short (below 10 ms) causing the signal to decay before detection. A shortening of the T_2 could also be due to internal gradients caused by the difference in susceptibility between water and air. T_2 maps were also recorded with a shorter echo time of 5 ms (data not shown) with similar results suggesting that internal gradients might have less impact on the obtained T_2 values. An echo time of 15 ms was chosen to ensure to capture long T_2s which are present in our samples. It is important to note that the spatial resolution is 312.5 µm and a swelled particle is most likely on a similar length scale but due to the irregular shape of the particles and the slice thickness of 1 mm; the voxels

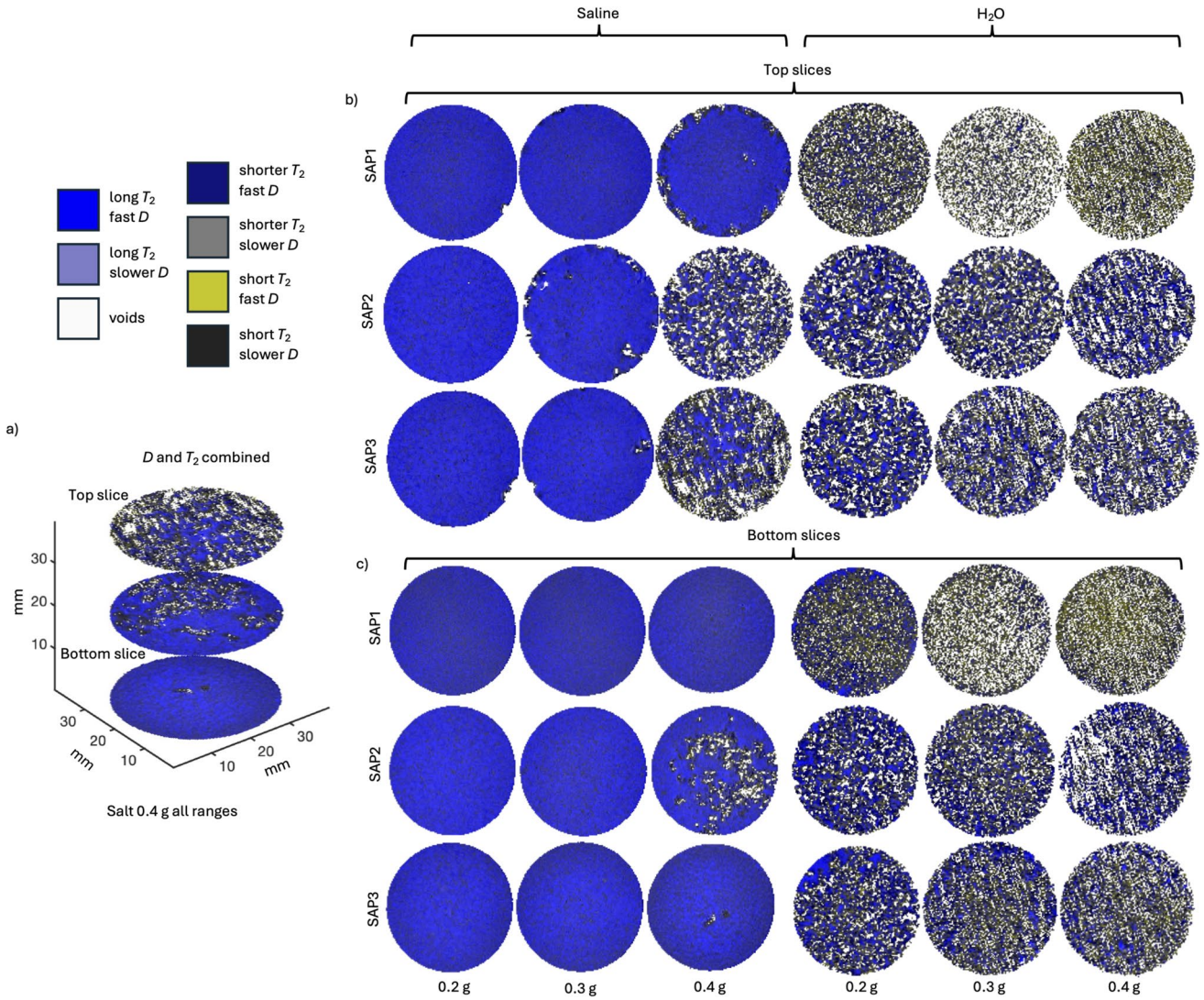

Figure 4 **a** Expanded view of D and T_2 map, showing top, middle, and bottom slice **b** top and **c** bottom slices shown of overlayed D and T_2 maps of either saline or water, at all SAP concentrations and SAP1, SAP2, and SAP3; colour code shown to the left top

may also have contributions from H_2O molecules between the particles. For saline swelled top slices, largest changes are seen at the highest concentration and largest particle sizes (SAP2 and SAP3), which look more like SAP swelled with water, i.e. with voids.

Previous studies [39, 40] have shown that particle size affects the performance of SAPs, with the specific impact depending on SAP structure, monomer composition, polymerisation process, and both degree and type of cross-linking [25]. For water swelled SAP, all slices, whether bottom or top, show distinct differences in the overlayed maps between particle sizes. Smaller particles have a higher surface area-to-volume ratio, providing an increased surface for H_2O molecules to enter the SAP particles, thereby shortening the distance required for an H_2O molecule to reach the particle core. This could result in a faster swelling process and/or a complete swelling in the same time frame compared to larger particles.

For the smallest particle size range (SAP1) swelled in H_2O and the lowest SAP concentration, there are almost no bright blue regions visibly attributed to fast D and long T_2. This indicates that most of the H_2O molecules are inside the swelled particles. With increasing SAP concentrations, there are mainly grey and yellow regions with moderately restricted H_2O diffusion and intermediate T_2 relaxation times. With increasing particle size (SAP2 and SAP3), bright blue

regions become visible showing that there are H_2O molecules between the swelled particles that have not been completely absorbed. Hence, the question arises; if the smallest particle size absorbs most of the water, what is limiting the absorption of water for larger particle sizes?

From the overlayed maps in Fig. 4, we can clearly see that there are voids between the swelled particles indicating empty space. As there is no solution in these areas, the SAP particles are not able to swell further. Also, larger particles could swell less or swell more heterogeneously, for example less swelling might occur in the core of the particle compared to the edges. A visual inspection of the overlayed maps for SAP2 and SAP3 swelled in H_2O does not show large differences in H_2O molecule distribution, indicating that for particle sizes larger than 300 μm, H_2O molecules which are close to the SAP particle surface may not become absorbed completely and stay between the swelled particles. Sweijen et al. developed a model for diffusion of H_2O in an SAP particle reporting on very fast water uptake kinetics with diffusion being the limiting factor [41]. This observation agrees with our results showing a larger water uptake for the smallest particle size.

To elucidate the impact of particle size on water or saline solution uptake, we employed 1D ^1H profiling which allowed for 130 ms temporal resolution. A 1D ^1H profile reports the sum of ^1H signal over a slice thickness of 1 mm for each position in the z-direction along the sample. The width of these profiles corresponding to the sample height with time is shown in Fig. 5. Each experiment uses 0.5 g of SAP and 10 ml of either solution. For both water and saline solution, the fluid uptake was the fastest for the smallest particle size SAP1 (black, top, and bottom). The slowest uptake was observed for the largest particle size SAP2 (blue, top, and bottom) and as expected, SAP3 (green, top and bottom), which includes both particle sizes, resulted in a medium uptake. These results also corroborate that water uptake is faster compared to saline solution. For the smallest particle size, SAP1, the uptake process appeared finished after 1 min while for saline solution, it takes 3 min. SAP particles swelled in water resulted of a difference in sample height of roughly 7 mm while for saline the sample height varied from 3 to 4 mm at the end of the experiment.

Maps as shown in Fig. 4 offer a visual assessment, but for a detailed comparison between SAP particle sizes and water and saline conditions, the maps were converted to distribution curves showing the range of T_2s and Ds. Distribution curves of normalised diffusion coefficient D and T_2 maps are shown in Fig. 6; they exclusively display the distributions of the top slices within the sample holder at various SAP particle sizes and concentrations, either in water or saline solution. This allows us to further investigate heterogeneity and understand the behaviour of H_2O molecules within the SAP material. A comparison of three slices is provided in Fig. 6 investigating the moments of the distributions.

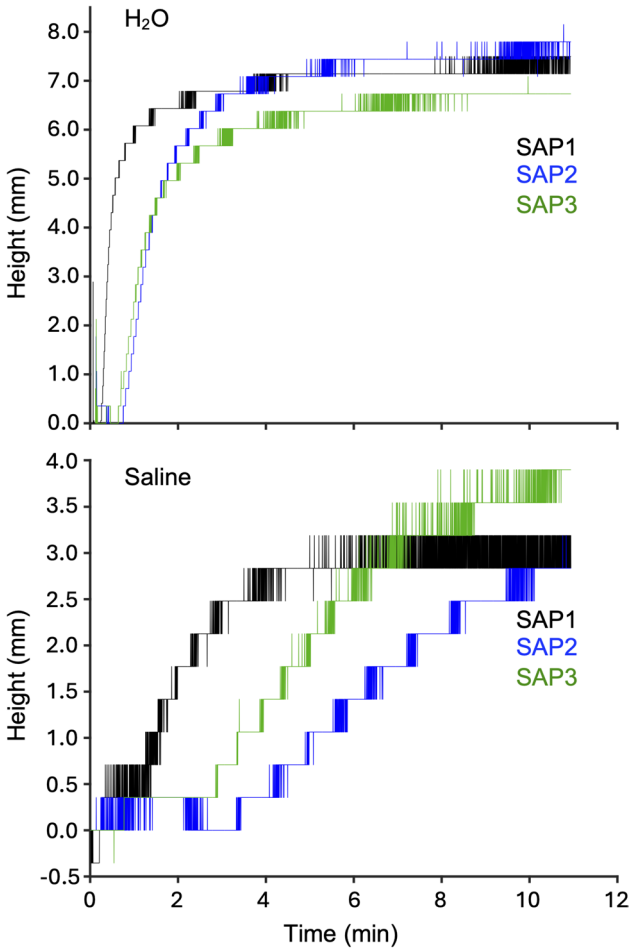

Figure 5 The swelling height in mm as a function of time for 0.5 g SAP particles (SAP1, SAP2, and SAP3) for water (top) and saline (bottom)

In saline swelled SAP maps, the normalised Ds mostly show a uniform Gaussian curve, due to increased presence of H_2O molecules between the swelled particles, while the normalised T_2s display a less Gaussian like distribution, particularly for SAP2 and SAP3. The most apparent difference is seen at the

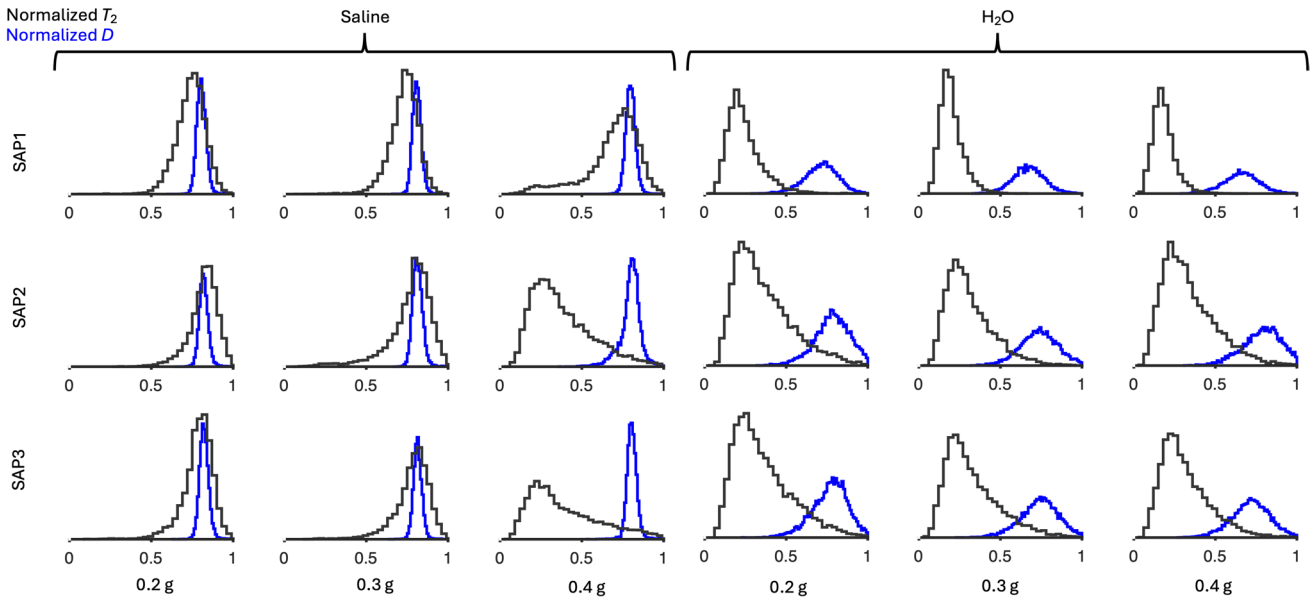

Figure 6 Example distribution plots shown of normalised D (blue) and T_2 (black) for SAP concentrations (0.2, 0.3, or 0.4 g), and particle sizes (SAP1, SAP2, and SAP3), separated into SAP swelled in either saline or water for top slices; normalised measurements to their respective solutions, saline, or water; and scaled relative to the total distribution

highest SAP concentration of 0.4 g. Here, at all particle sizes there is a marked difference in T_2 distribution, and at SAP2 and SAP3, there is a left sided, long tailed distribution for T_2, indicating heterogeneity and an increase in shorter T_2 times. This occurs due to a wider spread in T_2 relaxation times, and a heterogeneity due to voids being formed (see Fig. 4).

Water swelled SAP distributions display different trends to saline, for example, there is a right sided trend for all normalised T_2, corresponding to longer T_2 times. The distribution of the T_2s and Ds is much broader in comparison with the saline samples, indicating that the water swelled SAP particles are swollen heterogeneously. This could be due to the manufacturing process of the SAP particles, the swelling process, or the time frame during which the H_2O molecules are able to enter the SAP particles. The T_2 distributions appear to be the smallest for the smallest particle size (SAP1) for water swelled SAP which agrees with an earlier observation that these particles are most likely swelled homogenously compared to the particle sizes SAP2 and SAP3.

For increasing SAP concentration, a contribution with longer T_2s is observed which arises from the H_2O molecules between the SAP particles (bright blue regions in Fig. 4). However, the T_2s are in general shorter for the water swelled samples when compared to saline samples. This could be due to the hydrogen exchange rate on the $COOH/COO^-$ groups being slower or faster due to the presence of sodium ions not impacting the relaxation time T_2. It is however notable that for the particle size SAP2 and 0.4 g of SAP, short T_2s were observed. Another reason for the longer T_2s in the saline samples could be the contribution of H_2O molecules between the particles.

These distributions were further analysed using three of the four moments of distribution (Fig. 7). The mean and variance are raw moments, and the skewness and kurtosis are normalised/standardised moments (normalised with standard deviation). The latter are dimensionless. This research will not present the second moment of distribution, variance, as we did not observe any trends or patterns in data for this moment.

As seen in Fig. 7, the first moment of distribution, the mean, representing the average of the D and T_2 plots, shows clear patterns which are consistent between different SAP concentrations. In T_2 measurements, the saline solution consistently has a higher mean than water, for all slices and concentrations. For 0.4 g SAP concentration and SAP2 and SAP3 particle sizes, a clear difference is observed between all three slices. This could be explained as follows: bottom layer SAP particles, swelled by H_2O molecules, are expanding and pushing up the upper layers of SAP particles before the latter are completely swollen. These upper

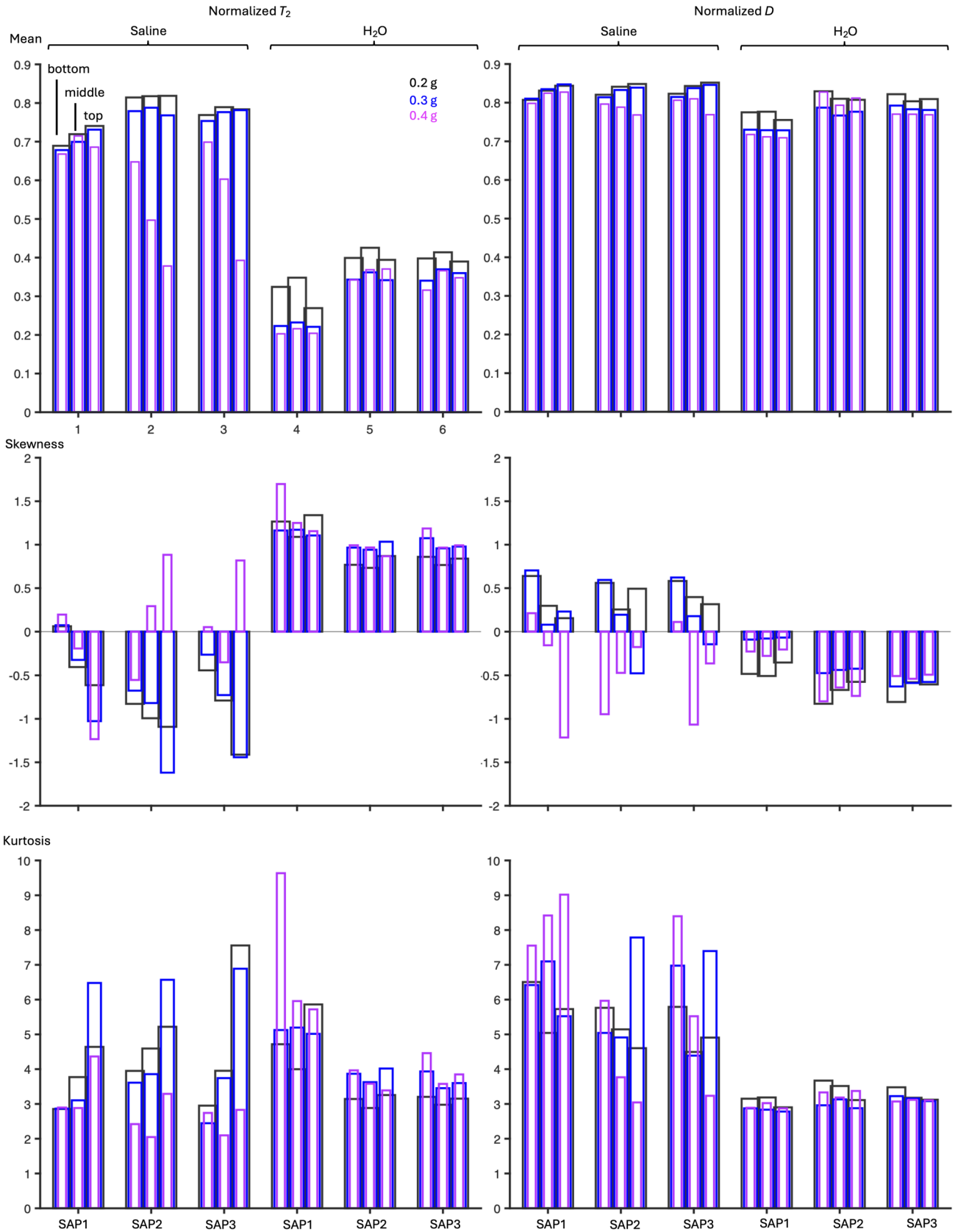

Figure 7 T_2 and D mean, skewness, and kurtosis of SAP1, SAP2, and SAP3 for SAP concentrations: 0.2, 0.3, and 0.4 g and coloured according to the key shown in top left bottom (b), middle (m), and top (t) slices arranged in triplicate, in that order, for each particle size

layers are then no longer in contact with 'free' solution, and therefore may not experience total swelling leading to a disparity of swelling between slices.

The third moment, skewness, represents a measure of asymmetry of the data around the sample mean. The skewness of a normal distribution is 0. If it spreads to the left, the skewness is negative; if it spreads to the right, the skewness is positive. There is a general trend of positive skewness for T_2 water measurements, correlating with having lower T_2 mean values. The skewness is negative for high mean values as for most of the T_2 saline measurements, while becoming positive at higher SAP addition also correlating with the lower T_2 mean values. In the saline samples, this might be due to more H_2O molecules being inside the SAP particles, and therefore, the contribution of the H_2O molecules between the particles becomes less. For the water swelled samples, the general trend is the opposite, as more H_2O molecules are present in between the particles pushing the distribution to longer T_2 values.

The fourth and final moment, kurtosis, is a measure of how outlier-prone a distribution is and has a value of 3 for a normal distribution. When a distribution is more prone to outliers, it will have a kurtosis of greater than 3, and vice versa. In this research, all outliers due to fitting errors have been screened out prior to analysis. 0.2 and 0.3 g of saline swelled SAP show an increase in kurtosis from the bottom to the top slice of T_2. This is not replicated for T_2, water swelled SAP, which shows less difference between slices, for 0.2 and 0.3 g SAP concentrations. These results indicate T_2 saline measurements are more prone to a spatial heterogeneity than other slices presented. This has previously been observed in Fig. 4. When water is present rather than saline, there is a more uniform, homogenous distribution between all slices, and kurtosis values are at around 3, hinting at a normal distribution, further reinforced by Fig. 6 which demonstrates a more normal distribution.

Consistent differences in heterogeneity have been observed between saline swelled SAP, and water swelled SAP. Saline ions may interact with charged groups on the polymer chains and may not distribute evenly throughout the polymer network. Particularly for the regions where the saline solution is no longer in contact with the SAP particles in comparison with regions where SAP particles are still covered by the saline solution. This uneven distribution can create areas with different hydration levels and relaxation time properties, which can lead to spatial heterogeneity in T_2 and D. In pure water, SAP could absorb and swell relatively uniformly due to a lack of ionic competition of sodium ions, from both the solution and the sodium neutralised SAP. This results (if the residence time of H_2O molecules close to the SAP matrix allows absorption), in a more homogenous polymer–H_2O matrix with consistent H_2O movement and relaxation. However, in the presence of saline, osmotic pressure is reduced, and non-specific interactions, such as electrostatic interactions, van der Waals forces, and hydrogen bonding, may limit the swelling of the SAP. Some regions may absorb more water while others remain less swelled, creating heterogeneity in H_2O movement and relaxation.

Conclusions

This work has highlighted the importance of the application of MRI and subsequent analysis techniques to look in depth at the absorption processes in absorbent structures. It shows, in a comparable manner, the position of water and its state in terms of free or strongly associated. The analytical measurements and representative maps of multiple fluid distributions were proved to shed light on important variables in fluids absorption in a bed of gelling particles.

Saline samples display heterogeneity throughout the sample slices, across varying SAP particle sizes and concentrations, while water swelled SAP maintains a more consistent spatial H_2O molecule distribution. The difference in the spatially distributed H_2O molecules is crucial for hygiene product applications aiming for fluids to be properly absorbed. Furthermore, we observed that a smaller particle size led to a faster fluid uptake.

The higher heterogeneity in water distribution in the saline swelled SAP samples can be explained by the lower absorption capacity in saline solution versus pure water which is a fact for the investigated superabsorbents. The fluid is usually absorbed into SAP particles it is in direct contact with. However, due to gravity and there being a finite volume of solution, these free H_2O molecules were mainly contained in the bottom layers. This could have led to less swelled particles at the top of the sample and remaining free liquid at the bottom of the sample. Results indicate a smaller particle size seems beneficial for a higher absorption of liquid.

It is important to note that although we have found these trends with these specific SAP particles, the same trends will not be applicable to all SAP. There is a vast range of particle formulations, sizes,

and co-polymers which ultimately affect absorbability and function. Further research will focus on applying herein presented MRI pulse sequences and subsequent analyses, to investigate the impact of stress conditions such as repeated solution application and pressure changes on swelled SAP particles.

Acknowledgements

We would like to thank the Bo Rydin foundation for financial support (F 11/21).

Funding

Open access funding provided by Chalmers University of Technology. Bo Rydins Stiftelse för Vetenskaplig Forskning,F 11/21,Diana Bernin.

Data availability

The data will be made available upon request. This is an experimental study, and no code has been developed.

Declarations

Conflict of interest The authors declare no conflict of interest.

Ethical approval Not applicable to our work as no humans or animals have been involved.

References

[1] Chidiac SE, Mihaljevic SN, Krachkovskiy SA, Goward GR (2021) Efficiency measure of SAP as internal curing for cement using NMR & MRI. Constr Build Mater 278:122365

[2] SR Benjamin, EJMR Júnior (2023) Tuteja J (ed) Properties and applications of superabsorbent polymers, Springer, Singapore, pp 183–199

[3] Lejcus K, Spitalniak M, Dabrowska J (2018) Swelling behaviour of superabsorbent polymers for soil amendment under different loads. Polymers 10:271

[4] Bachra Y, Grouli A, Damiri F, Bennamara A, Berrada M (2020) A new approach for assessing the absorption of disposable baby diapers and superabsorbent polymers: a comparative study. Results Mater 8:100156

[5] GV Research (2024) Super absorbent polymer market size, share & Trends analysis report 2024–2030. Databook H https://www.researchandmarkets.com/reports/4613437/super-absorbent-polymer-market-size-share-and

[6] Pourjavadi A, Harzandi AM, Hosseinzadeh H (2004) Modified carrageenan 3. synthesis of a novel polysaccharide-based superabsorbent hydrogel via graft copolymerization of acrylic acid onto kappa-carrageenan in air. Eur Polym J 40:1363–1370

[7] Qin X, Lin Y, Mao J, Sun X, Xie Z, Huang Q (2023) Research of water absorption and release mechanism of superabsorbent polymer in cement paste. Polymers 15:3053

[8] Nott KP (2010) Magnetic resonance imaging of tablet dissolution. Eur J Pharm Biopharm 74:78–83

[9] Mukhatov A, Le TA, Pham TT, Do TD (2023) A comprehensive review on magnetic imaging techniques for biomedical applications. Nano Sel 4:213–230

[10] Serai SD, Trout AT, Fleck RJ, Quinn CT, Dillman JR (2018) Measuring liver T2* and cardiac T2* in a single acquisition. Abdom Radiol 43:2303–2308

[11] Serai SD, Fleck RJ, Quinn CT, Zhang B, Podberesky DJ (2015) Retrospective comparison of gradient recalled echo R2* and spin-echo R2 magnetic resonance analysis methods for estimating liver iron content in children and adolescents. Pediatr Radiol 45:1629–1634

[12] Traub TFB, Hafner S, Spiess HW (1999) Characterization of superabsorbing polymers by NMR imaging. Colloid Polym Sci 2000:547–552

[13] Kazemian M, Shafei B (2024) Investigation of type, size, and dosage effects of superabsorbent polymers on the hydration development of high-performance cementitious materials. Constr Build Mater 422:135801
[14] Guo X, Theissen S, Claussen J et al (2018) Dynamics of sodium ions and water in swollen superabsorbent hydrogels as studied by 23Na- and 1H-NMR. Macromol Chem Phys 220:1800350
[15] Fang S, Wang G, Li P et al (2018) Synthesis of chitosan derivative graft acrylic acid superabsorbent polymers and its application as water retaining agent. Int J Biol Macromol 115:754–761
[16] Guo X, Theissen S, Claussen J et al (2018) Topological insight into superabsorbent hydrogel network structures: a 1H double-quantum NMR study. Macromol Chem Phys 219:1800100
[17] Qi Z, Hu X (2022) Water absorbency of super absorbent polymer based on flexible polymeric network. Eur Polym J 166:111045
[18] Zhang M, Zhang S, Chen Z, Wang M, Cao J, Wang R (2019) Preparation and characterization of superabsorbent polymers based on sawdust. Polymers 11:1891
[19] Misiewicz J, Lejcus K, Dabrowska J, Marczak D (2019) The characteristics of absorbency under load (AUL) for superabsorbent and soil mixtures. Sci Rep 9:18098
[20] Bachra Y, Grouli A, Damiri F, Zhu XX, Talbi M, Berrada M (2022) Synthesis, characterization, and swelling properties of a new highly absorbent hydrogel based on carboxymethyl guar gum reinforced with bentonite and silica particles for disposable hygiene products. ACS Omega 7:39002–39018
[21] Mohebbi B, Claussen J, Blumich B (2019) Fast and robust quantification of liquid inside thin fibrous porous materials with single-sided NMR. Magn Reson Imaging 56:131–137
[22] Mohebbi B, Tavangarrad AH, Claussen J, Blumich B, Hassanizadeh SM, Rosati R (2018) Revealing how interfaces in stacked thin fibrous layers affect liquid ingress and transport properties by single-sided NMR. J Magn Reson 294:16–23
[23] Pell GS, Landeryou MA, Cottenden AM, Ordidge RJ (2003) NMR investigation of the nature of water in disposable incontinence pads containing superabsorbent polymers and fluffed wood pulp. Colloid Polym Sci 281:1127–1135
[24] Doll KM, Vermillion KE, Fanta GF, Liu Z (2012) Diffusion coefficients of water in biobased hydrogel polymer matrices by nuclear magnetic resonance imaging. J Appl Polym Sci 125:E580–E585
[25] Yang YY, Liang ZY, Zhang R et al (2024) Research advances in superabsorbent polymers. Polymers 16:501
[26] Mahon R, Balogun Y, Oluyemi G, Njuguna J (2019) Swelling performance of sodium polyacrylate and poly(acrylamide-co-acrylic acid) potassium salt. SN Appl Sci 2:117
[27] Chenhao Zhao MZ, Liu Z, Guo Y, Zhang Q (2019) Salt-tolerant superabsorbent polymer with high capacity of water nutrient retention derived from sulfamic acid-modified starch. ACS Omega 3:5923–5930
[28] Mechtcherine V, Snoeck D, Schroefl C et al (2018) Testing superabsorbent polymer (SAP) sorption properties prior to implementation in concrete: results of a RILEM round-robin test. Mater Struct 51:1–16
[29] S Pradhan, S Pradhan (2023) Pradhan S, Mohanty S (eds) Bio-based superabsorbents: recent trends, types, applications and recycling, Springer Nature Singapore, Singapore, pp 67–75
[30] Chavhan GB, AlSabban Z, Babyn PS (2014) Diffusion-weighted imaging in pediatric body MR imaging: principles, technique, and emerging applications. Radiographics 34:E73–E88
[31] O'Donnell LJ, Westin CF (2011) An introduction to diffusion tensor image analysis. Neurosurg Clin N Am 22:185–196
[32] Kharbanda Y, Urbanczyk M, Laitinen O et al (2019) Comprehensive NMR analysis of pore structures in superabsorbing cellulose nanofiber aerogels. J Phys Chem C 123:30986–30995
[33] Hamuro Y (2021) Tutorial: chemistry of hydrogen/deuterium exchange mass spectrometry. J Am Soc Mass Spectrom 32:133–151
[34] Santos RVA, Costa GMN, Pontes KV (2019) Development of tailor-made superabsorbent polymers: review of key aspects from raw material to kinetic model. J Polym Environ 27:1861–1877
[35] Jangizehi A, Fengler C, Arens L, Wilhelm M (2020) Optimizing the power production in an osmotic engine via microfluidic fabricated and surface crosslinked hydrogels utilizing fresh and salt water. Macromol Mater Eng 305:2000174
[36] Arens L, Weissenfeld F, Klein CO, Schlag K, Wilhelm M (2017) Osmotic engine: translating osmotic pressure into macroscopic mechanical force via Poly(Acrylic Acid) based hydrogels. Adv Sci 4:1700112
[37] Namazi H, Hasani M, Yadollahi M (2019) Antibacterial oxidized starch/ZnO nanocomposite hydrogel: synthesis and evaluation of its swelling behaviours in various pHs and salt solutions. Int J Biol Macromol 126:578–584
[38] Lenji MA, Haghshenasfard M, Sefti MV, Salehi MB, heidari A (2018) Experimental study of swelling and rheological behavior of preformed particle gel used in water shutoff treatment. J Petrol Sci Eng 169:739–747

[39] Adsul N, Lee JW, Kang ST (2024) Investigating the impact of superabsorbent polymer sizes on absorption and cement paste rheology. Materials Basel 17:3115
[40] Yang H, Liu M, Bian H, Wu L, Liu J, Wang W (2022) The influence of SAP particle size and extra water on the dynamic mechanical behavior of SAP-modified cement-based composites. Constr Build Mater 347:128622
[41] Sweijen T, van Duijn CJ, Hassanizadeh SM (2017) A model for diffusion of water into a swelling particle with a free boundary: application to a super absorbent polymer particle. Chem Eng Sci 172:407–413